LAWRENCE
LIVERMORE
NATIONAL
LABORATORY

LLNL-JRNL-404373

Ultra-fast x-ray Thomson scattering measurements of insulator-metal transition in shock-compressed matter

A. Kritcher, P. Neumayer, J. Castor, T. Doppner, R. W. Falcone, O. L. Landen, H. J. Lee, R. W. Lee, E. C. Morse, A. Ng, S. Pollaine, D. Price, S. H. Glenzer

June 2, 2008

Science

Disclaimer

Ultra-fast x-ray Thomson scattering measurements of insulator-metal transition in shock-compressed matter

Andrea L. Kritcher[1,2], Paul Neumayer[2], John Castor[2], Tilo Döppner[2], Roger W. Falcone[3], Otto L. Landen[2], Hae Ja Lee[3], Richard W. Lee[2,3], E. C. Morse[1], Andrew Ng[2], Steve Pollaine[2], Dwight Price[2], Siegfried H. Glenzer[2]

[1]Nuclear Engineering Department, University of California Berkeley, Berkeley, CA 94709, USA. [2]Lawrence Livermore National Laboratory, P.O. Box 808, Livermore, CA 94551, USA. [3]Physics Department, University of California Berkeley, Berkeley, CA 94709, USA. [†]Corresponding author; kritcher@berkeley.edu

Spectrally resolved scattering of ultra-short pulse laser-generated K-α x rays has been applied to measure the heating and compression of shocked solid-density lithium hydride. Two shocks launched by a nanosecond laser pulse coalesce yielding pressures of 400 gigapascals. The evolution of the intensity of the elastic (Rayleigh) scattering component indicates rapid heating to temperatures of 25,000˚K on a 100 ps time scale. At shock coalescence, the scattering spectra show the collective plasmon oscillations indicating the transition to the dense metallic plasma state. The plasmon frequency determines the material compression, which is found to be a factor of three thereby reaching conditions in the laboratory important for studying astrophysics phenomena.

Shock wave heating is a key technique to produce matter at extreme conditions in the laboratory where the physics of planetary formation (1) and modeling of planetary composition (*2*) can be tested. Contemporary experiments are designed to determine the equation of state (EOS) of light elements (*3-5*) or measure effects of shock waves on matter, for example to investigate effects by solar nebula shocks (*6*). In addition, the inertial confinement approach to controlled nuclear fusion (*7*), employs a deuterium-tritium filled capsule that will be compressed to 1000 times solid density and heated to temperatures larger than the interior of the sun using a sequence of coalescing shock waves.

Previous shock wave experiments have been restricted to measuring particle and shock velocities (*4*). The experiments reported here have directly measured the thermodynamic properties and dynamic structure factors of shocked matter. These novel experiments have only now become possible with the advent of penetrating powerful x-ray probes (*8*) produced by high-energy (300 J) petawatt-class ultra-short pulse lasers. This work provides the first experimental validation of modeling of compression and heating of shocked matter with an unprecedented temporal resolution of approximately 10 ps. These measurements are important since calculating the conditions of shocked matter requires knowledge of the equation of state (EOS), that in turn require many body physics solutions.

In this study, we have shock-compressed lithium-hydride, LiH, with an energetic nanosecond laser and have measured the conditions with spectrally-resolved x-ray Thomson scattering (*9-11*). These pump-probe experiments show that efficient compression and heating occurs at temperature and density conditions previously not accessible to quantitative *in situ* characterization. The experimental data show a factor of three compression with concomitant heating to T = 25,000˚K = 2.2 eV in broad agreement with radiation-hydrodynamic modeling. While the range of temperature traversed in phase space by shock compression agree with calculations that use a quotidian *(12)* equation-of state (QEOS), calculations with the Sesame *(13)* EOS tables provide a better match of the coalescence time.

Figure 1 (a) shows the schematic of the experiment together with a data record from the x-ray spectrometer. A 400-J laser beam from the Titan laser facility at the Lawrence Livermore National Laboratory *(14)* irradiates 300 μm thick LiH (initial density of ρ_0 = 0.78 g/cc). The laser pulse was shaped in time (Fig. 1 (b)) having a 4 ns-long foot with laser intensity of 10^{13} W/cm^2 followed by a 2 ns-long peak at $3\text{x}10^{13}$ W/cm^2. Figure 1 (c) shows a result of radiation-hydrodynamic simulations (*15*) indicating that two shock waves have been launched into the target that coalesce and compress the target to 2.2 g/cc about 7 ns after the beginning of the laser drive.

An ultra-short pulse laser delayed from the nanosecond laser illuminates a titanium foil producing a 10 ps-long K-α x-ray pulse (*16*) at an x-ray energy of E_0 = 4.51 keV that penetrate through the dense compressed LiH. By varying the delay between the nanosecond heater beam and the short pulse probe beam, conditions before and during shock coalescence are probed. The short pulse laser energy of 300 J is converted to Ti K-α with an efficiency of 5×10^{-5} providing 10^{12} x-ray photons on target sufficient for measurements of elastic and inelastic scattering components in a single shot. The spectrometer consists of a large 25x70 mm^2 curved graphite (HOPG) crystal *(17)* in van Hamos geometry *(18)* and in the mosaic focusing mode *(9)* that diffracts the signal for scattering angles in the range of $\theta = 40^\circ \pm 10^\circ$ onto an Imaging Plate (IP) detector.

The data record at shock coalescence shows features in the scattering spectrum due to interactions with the delocalized, i.e. metallic, and bound electrons; the former undergo plasma (Langmuir wave) *(19)* oscillations at the plasma frequency that give rise to the inelastic plasmon scattering feature *(11)* while the latter give rise to elastic Rayleigh scattering *(9)*.

The plasmon feature is downshifted from the incident 4.51 keV x rays as determined by the Bohm Gross dispersion relation *(20)* with the leading term being the plasma frequency, $\omega_p = (n_e e^2/\varepsilon_o m_e)^{1/2}$. Here, n_e is the electron density, ε_o the permittivity of free space, e and m_e the electron charge and mass, respectively. Thermal corrections due to the propagation of the oscillations are small, while quantum diffraction is calculated from the Compton energy, $E_C = (h/2\pi)^2 k^2/2m_e$ = 9.3 eV. Here, h is Planck's constant and the scattering vector **k** that determines the scale length of electron density fluctuations depends only on the probe energy and scattering angle, $k = 4\pi (E_0/hc) \sin(\theta/2) = 1.6$ Å^{-1}. Thus, the downshift of the plasmon provides the electron density.

The strongly bound K-shell electrons of Li and H that interact with x-ray photons are not excited by the scattering process as their ionization potential is less than the Compton energy, therefore resulting in elastic scattering events. The intensity is sensitive to the number of strongly bound electrons and the ion-ion structure factor; the latter is sensitive to the ion temperature. Hence, the temperature can be inferred from the elastic scattering strength.

Figure 2 shows the experimental scattering spectrum at shock coalescence at t = 7 ns and at t = 4 ns exactly before the second strong shock wave has been launched. These spectra are fit with calculated scattering

profiles using the theoretical dynamic form factor of Gregori *(21)*. Also shown is a spectral profile of the Ti K-α source measured with the same spectrometer. In addition to the short probe pulse duration required to time-resolve the shock wave coalescence, this x-ray source exhibits no spectral features on the red wing of the K-α doublet allowing accurate observations of inelastic scattering on plasmons.

The scattering signal at t = 4 ns shows only elastic scattering indicating a lack of free electrons. The theoretical fit that takes into account contributions from bound and fee electron limits the degree of ionization to $Z^* < 0.1$. However, the intensity of the elastic scattering peak alone has increased by 40%±10% compared to scattering from cold samples indicating a temperature of 0.2 eV.

In contrast, when the shock waves coalesce at t = 7 ns, strong plasmon oscillations give rise to inelastic scattering downshifted from the elastic peak by ΔE_{pl} = 25 eV. In this case, the material is ionized with $Z^*=1$ for $Li^{(+)}H$. The elastic scattering signal has increased by 100%±10% compared to scattering from cold samples indicating temperatures of 2.2 eV.

For the degenerate systems encountered here, the plasma screening length, λ_S, at which local electric fields are shielded by mobile charge carriers, is approaching the Thomas-Fermi length, resulting in λ_S = 0.57 Å *(21)*. Therefore, scattering is collective with a scattering parameter *(22)*, $\alpha = 1/k\lambda_S$ = 1.1 where the scattering scale length is of order of the screening length required for observations of plasmon oscillations.

The plasmon shift determined by the calculated spectra provides the electron density of $n_e = 1.7 \times 10^{23}/cm^3$. This calculation includes the thermal corrections including degeneracy and from quantum diffraction. The density is obtained with an error of 10% due to noise in these single shot data. Accurate knowledge of the electron density further determines the absolute electron-electron structure factor *(23)*. In the long-wavelength limit

$$S_{aa}(k) = k^2/(k^2 + \lambda_S^{-2}) \quad (1)$$

with a= e, i for electron or ions. With λ_S for a partly degenerate electron fluid, we find $S_{ee}(k)$ = 0.46. This value combined with the measured elastic and inelastic scattering amplitude thus determines the absolute ion-ion structure factor, which yields the ion temperature from the ion Debye screening length. The spectral calculations and parameters of Fig. 2 include multiple-species ion-ion structure factors from one-component electron-ion interaction potentials *(24)* that have been shown to be consistent with previous experiments *(11)*.

Figure 3 shows the evolution of the measured temperature as function of time along with the results from radiation-hydrodynamic calculations. The strong rise at t = 7 ns indicates coalescence of the shock waves. The temperature has been inferred with an error of 10-20% due to noise. In addition, corrections have been included to account for partial scattering from uncompressed material. Without this correction, the temperatures are about 10% higher.

The experimental temperature data and the timing of coalescence are in broad agreement with simulation. The ranges of temperatures shown in Fig. 3 are from calculations that include various amounts of impurities and oxide layers consistent with target characterization. The QEOS being the simpler model includes a modified electronic Thomas–Fermi statistical model with ion thermal motion calculated beyond the Grüneisen EOS by including temperature-dependent corrections to the pressure. This model is consistent with the wide range of temperatures accessed in this experiment.

The Sesame EOS includes atomic structure based on solutions of the single particle quantum levels in the self-consistent field of an atom *(25)*. The peak temperature and the experimentally observed coalescence time are in excellent agreement with modeling that uses the Sesame EOS. On the other hand, using Sesame results in less satisfactory agreement early in time indicating that a future comparison with *first-principles* statistical models *(26)* will be of interest to understand these weakly shocked systems.

At peak temperature, the calculations indicate pressures in the range of P = 300 – 420 GPa. With $Z^* = 1$ and the electron density from the plasmon data we find a density of ρ = 2.25 g/cc corresponding to three times compressed LiH. Further, assuming that the shocks coalescence at about 120 μm (cf. Fig. 1(c)) provides the fast shock velocity, $u_s \sim 30$ km/s. This information combined with the Rankine-Hugoniot equations,

$$\rho/\rho_0 = u_s/(u_s - u_p) \quad (2)$$

$$P = \rho_0 u_s u_p \quad (3)$$

and with ρ_0 = 1.5 g/cc after the first shock, results in the particle velocity of $u_p = 1/3\ u_s$, and a pressure in the range of 300 to 400 GPa. These pressures agree with the radiation-hydrodynamic simulations and are consistent with the pressures at which Wang *(26)* predicted the insulator-metal phase transition.

In summary, we have demonstrated the capability to measure the temperature and density in dense matter during shock compression with 10 ps temporal resolution. The experiments have shown the transition to a metallic plasma state in the solid phase resulting in the observation of plasmons. This feature has further allowed testing of radiation-hydrodynamic calculations with different EOS models for shock-compressed matter. This technique is opportune for inertial confinement fusion experiments that will achieve extreme densities, e.g., on the National Ignition Facility *(27)*, which will require high temporal resolution for characterization of short-lived states of compression.

Finally, the K-α x-ray source employed in this study provides the same number of x-ray photons on target as projected for future x-ray free electron laser facilities (*28,29*). This indicates that x-ray Thomson scattering experiments on dense matter will soon be accessible for high repetition measurements of thermodynamic properties with 20-200 fs temporal resolution.

References and Notes

This work performed under the auspices of the U.S. Department of Energy by Lawrence Livermore National Laboratory under Contract DE-AC52-07NA27344. This work was further supported by DOE grant, NA-16 Intermediate Facility Initiative, by grants 08-ERI-002, 08-LW-004, and the Lawrence Scholar Program fellowship.

1. H. C. Connolly, Jr. *et al.,* Science **280**, 62 (1998).
2. T. Guillot *et al.,* Science **286**, 72 (1999).
3. N. C. Holmes *et al.*, Phy. Rev. B. **52**, (1995).
4. G. W. Collins *et al.,* Science **281**, 1178 (1998).
5. M. D. Knudson *et al.*, Phys. Rev. Lett. **87** (2001).
6. C. P. McKay *et al.,* Science **276**, 390 (1997).
7. J. D. Lindl *et al.,* Phys. Plasmas **11**, 339. 2004.
8. O. L. Landen *et al.,* Rev. Sci. Instrum. **72**, 627 (2001).
9. S. H. Glenzer *et al.,* Phys. Rev. Lett. **90**, 175002 (2003), *ibid* Phys. Plasmas **10**, 2433 (2003).
10. A. Racasio *et al.,* Phys. Rev. Lett. **99**, 135006 (2007)
11. S. H. Glenzer *et al.,* Phys. Rev. Lett. **98**, 065002 (2007)
12. R. M. Moore, K. H. Warren, D. A. Young, and G. B. Zimmerman, Phys. Fluids **31**, 3059 (1988).
13. S. Crockett, SESAME 7246, in Los Alamos National Laboratory Report No. LA-UR-06-8403.
14. P. Beiersdorfer, *et al.,* NIFS Proceedings Series No. NIFS-PROC-57, p. 40-46 (2004).
15. J. J. MacFarlane, *et al.,* JQSRT **99**, 381 (2006).
16. Chen, H., R. Shepherd, H. K. Chung *et al.,* Phys. Rev E **76**, 056402 (2007).
17. F. J. Marshall and J. A. Oertel, Rev. Sci. Instrum. **68**, 735 (1997).
18. M. K. Urry, G. Gregori, O. L. Landen *et al.,* J. Quant. Spectr. Rad. Trans. **99**, 636 (2006).
19. L. Tonks and I. Langmuir, Phys. Rev. **33**, 195 (1929).
20. D. Bohm and E. P. Gross, Phys. Rev. **75**, 1851 (1949).
21. G. Gregori *et al.,* Phys. Rev. E **67**, 026412 (2003).
22. J. Sheffield, Plasma Scattering of Electromagnetic Radiation (Academic Press, New York, 1975).
23. S. Ichimaru, Rev. Mod. Phys. **54**, 1017 (1982).
24. G. Gregori *et al.,* High Energy Den. Phys. **3**, 99 (2007).
25. D. A. Lieberman, Phys. Rev. B **20**, 4798 (1979).
26. T. Ogitsu, E. Schwegler, F. Gygi, a d G. Galli, , Phys. Rev. Lett. **91**, 175502 (2003).
26. Y. Wang, R. Ahuja, and B. Johansson, Phys. Stat. Sol. **235**, 470 (2003).

27. E. Moses and C. R. Wuest, Fusion Sci. Tech. **47**, 314-322 (20Ω05).
28. R. Akre, D. Dowell, P. Emma *et al.,* Phys. Rev. ST Accel. Beams **11**, 030703 (2008)
29. W. Ackermann, W., G. Asova, V. Ayvazyan *et al.,* Nature Photonics **1**, 336 (2007).

Supporting Online Material
www.sciencemag.org
Materials and Methods

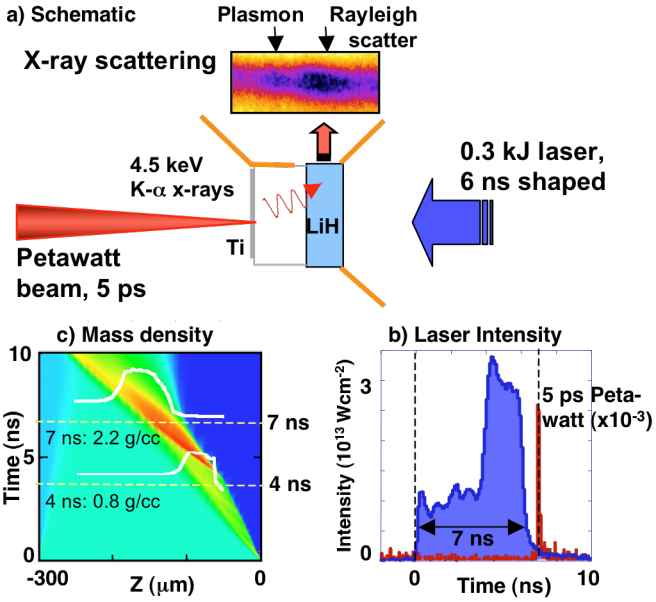

Fig. 1: (a) Schematic of experimental setup. A short (10 ps), mono-energetic (ΔE/E < 0.5%), x-ray probe is generated by ultra short-pulse laser irradiation of a titanium foil. The 10^{12} photons emitted from the foil interact with matter compressed by the nanosecond-long shaped laser pulse. The x-ray Thomson scattering spectrum shows inelastic scattering on plasmons and elastic Rayleigh scattering features. (b) The evolution of the shocks is measured at various times by changing the delay between the ultra short pulse laser probe and the long-pulse pump beam. (c) Radiation hydrodynamic modeling indicate coalescence of the shock waves at t = 7 ns.

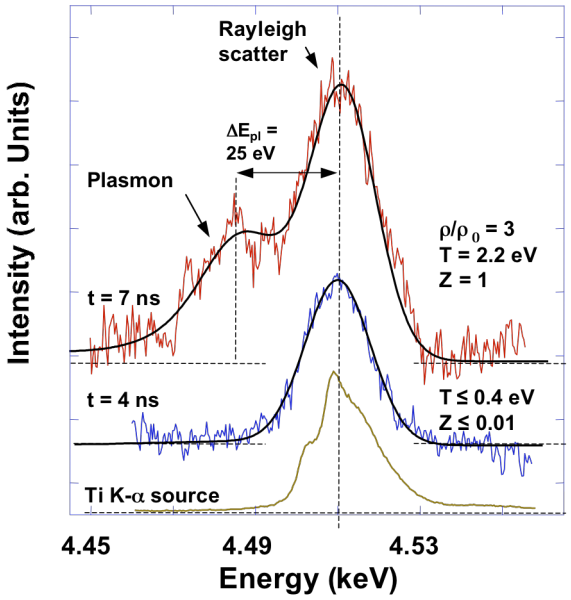

Fig. 2: X-ray scattering spectrum from shocked LiH indicating elastic Rayleigh scattering and inelastic plasmon scattering features. At t= 7 ns (top), the plasmon energy shift of 25 eV indicates compression of 3, while the intensity of the elastic scattering shows heating to temperatures of 2.2 eV. Earlier in time only elastic scattering is observed (middle) as demonstrated when compared with the K-α source spectrum (bottom). The observation of plasmons at t = 7 ns indicates the transition to the metallic free electron plasma in the solid phase.

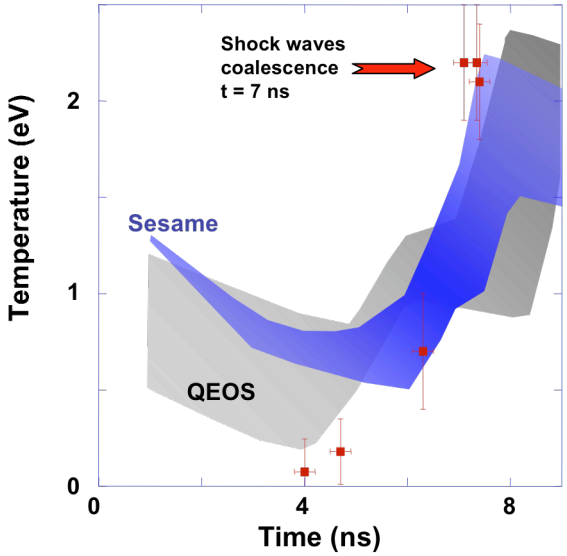

Fig. 3: The temperature of the shocked LiH is shown as function of time from the x-ray Thomson scattering measurements and from radiation-hydrodynamic modeling using different EOS models. The range of temperatures for each model is accounting for LiOH surface impurities (lower bounds) to no impurities (upper bounds). The experiments and calculations demonstrate efficient heating by shock coalescence with small differences in shock timing resolved by the short K-α x-ray pulses.